Acta Oto-Laryngologica, 2006; 126: 282–287

Taylor & Francis
Taylor & Francis Group

ORIGINAL ARTICLE

Particle image velocimetry measurements for the study of nasal airflow

JIN KOOK KIM[1], JOO-HEON YOON[2,3,4,5], CHANG HOON KIM[2,3], TAE WOOK NAM[1], DAE BO SHIM[1] & HYANG AE SHIN[1]

[1]*Department of Otorhinolaryngology—Head and Neck Surgery, Konkuk University College of Medicine, Seoul, Korea and* [2]*Department of Otorhinolaryngology,* [3]*The Airway Mucus Institute and* [4]*Brain Korea 21 Project for Medical Science and* [5]*Biomolecule Secretion Research Center, Yonsei University College of Medicine, Seoul, Korea*

Abstract

Conclusions. Particle image velocimetry (PIV) permits investigation of the distribution and velocity of the airflow in the nasal cavity. During breathing, the main laminar flow stream passes through the middle meatus and turbulent flow can be detected under physiologic conditions. *Objectives*. Physical models or casts of the nasal cavity have been utilized in several studies in an effort to understand its aerodynamics. PIV is a new technique for measuring the aerodynamic properties of tubular structures. In this article we evaluate nasal airflow characteristics during physiologic breathing under normal conditions and the usefulness of PIV. *Material and methods*. A nasal model cast obtained by a combination of rapid prototyping and solidification of clear silicone was connected to a pump which simulated the physiological pressure in the upper airway system. A glycerol–water mixture was used as the flow material. The airstream was marked with spherical polyvinyl particles, observed through solidified clear silicone and analyzed using PIV. *Results*. The main flow within the cavity, which was mostly laminar, passed through the middle meatus. Turbulence was clearly visible in the anteroinferior part of the middle turbinate. The flow rate was highest at the middle meatus during inspiration and expiration.

Keywords: *Aerodynamics, human model, nasal airflow, particle image velocimetry*

Introduction

The nose, as a constituent of the respiratory system, carries out a variety of functions, such as modulation of airflow transmission, optimization of the temperature and humidity of the inspired air and olfaction. The mucous-covered inferior, middle and superior meatus, which encompass a vast surface area, allow for the maximum amount of contact with air, which in turn facilitates heat supply, moisturization and filtration, as well as olfactory function. A concrete analysis of the aerodynamics within the nasal cavity is critical in order for these functions to be carried out optimally. Thus, an understanding of the airflow within the nasal cavity serves as a basis to explain the physiologic and pathologic events within it. This has prompted many physiologists and biomedical researchers to engage in intensive investigations. Although several investigators [1,2] recently carried out trials aimed at analytical visualization using the nasal cavity as the model, and some obtained valuable data by directly measuring the velocity of the airflow using hot-wire anemometry, they had difficulty visualizing the complex geometrical figures of the nasal cavity and designing the appropriate experimental setting. Those studies, performed using a highly simplified half-nose model, yielded conflicting results which varied with the degree of simplification and the method of measurement and failed to provide evidence that the airflow activates heat transmission, leading to turbulence.

Recently, the introduction by Hopkins et al. [3] of the rapid prototyping and liquid translucent silicone consolidation technique, which utilizes CT images, enabled us to model the complex internal anatomy of the nasal cavity using a rectangular-shaped air conduit. By allowing microscopic particles to flow within this conduit, we were able to observe the

Correspondence: Jin Kook Kim, MD, PhD, Department of Otorhinolaryngology—Head and Neck Surgery, Konkuk University College of Medicine, 1 Hwang-dong, Gwangjin-gu, Seoul 143-701, Korea. Tel: +82 2 2030 7661. Fax: +82 2 2030 7749. E-mail: jkkimmd@kuh.ac.kr

(Received 3 June 2005; accepted 18 August 2005)

ISSN 0001-6489 print/ISSN 1651-2551 online
DOI: 10.1080/00016480500361320

airflow within the cavity using particle image velocimetry (PIV). Using this method, we produced a model of half of the nasal cavity of South Korean subjects without nasal disease. Unlike previous models, which featured an almost horizontal inlet to the nasal floor [3,4], in this study we designed a model in which the inlet was curve-shaped and thus more compatible with the human anatomic structure, facilitating nasal airflow into the nasal vestibule under physiologic conditions. We measured the average airflow velocity during expiration and inspiration and its root mean square (RMS), which is calculated by taking the square root of the sum of the difference between the average velocity field and the instantaneous velocity at each point squared. A high value of the RMS of the average airflow velocity indicates a high velocity gradient at a certain point. In this study we analyzed and compared the patterns of nasal airflow using PIV, a new method for measuring the aerodynamics of the nasal cavity.

Material and methods

Creation of nasal model

The production of an accurate air conduit is the key to an effective and precise analysis of the airflow within the nasal cavity. For this purpose, we created a solid model for the air conduit within the nasal cavity using a rapid prototyping device (Z Corporation, Burlington, MA), which was fed with high-resolution CT (1-mm thick; 0.5 pixels) images obtained from healthy individuals who had not been treated with topical decongestants and had no nasal septal defects (Figure 1). The model reflected the area demarcated by the nasal vestibule anteriorly and the inferior margin of the nasopharynx posteriorly. Due to nasal cycle, the patency of the nasal cavities may be asymmetric. So we chose the more patent nasal cavity. We used water-soluble cornstarch as the primary construction material. After placing the model in an acryl box, we poured in a mixture of clear liquid silicone and sclerosing agent (both from Shin-Etsu Chemical Co., Tokyo, Japan) very carefully in order to avoid any bubble formation, and allowed it to solidify. During this process, we made sure no silicone leaked inside the cornstarch model by painting its surface several times with water-soluble glue, and the sclerosing agent was allowed to solidify by supplying an adequate amount of heat, which varied with the type of commercial model used. The flow conduit finally takes shape when the starch model is removed using cold water, after the silicone has completely solidified. Because the optical characteristics of a flow conduit obtained in this way differ from those of water and air, which is the reason why distortion of the image field is seen when water is used as a flowing material, we added glycerol to water (59% glycerol/41% water v/v; kinematic viscosity $= 6.55 \times 10^{-6}$ m^2/s at 27.5°C) [5] in order to obtain a glycerol concentration with the same refractory index as the conduit. According to Reynolds number-matching, when a kinematic viscosity of 16×10^{-6} m^2/s is used for air and a flow rate of 125 ml/s, which is a typical resting breathing rate, the necessary glycerol–water volume flow rate is 103 ml/s.

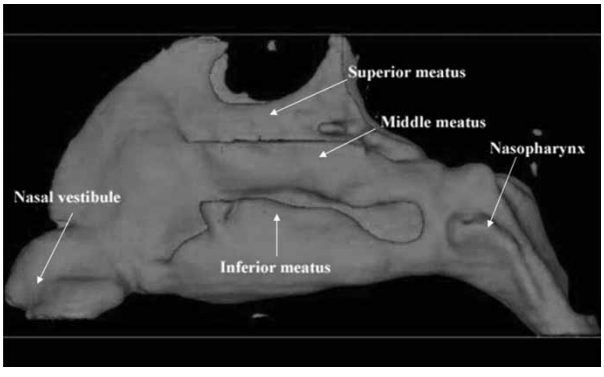

Figure 1. 3D reconstruction of the human nasal cavity using CT images.

PIV algorithms

The underlying principle of visualization of flow using PIV is as follows. We trace the movement of particles placed in the flow field, record their images at 1-min intervals and export them to an image processing device. We then measure the velocity variance of each of the particles and calculate the velocity vector within the entire field. Visualization of flow using PIV, in comparison to other standard methods such as laser Doppler velocimetry or hot-wire anemometry is more effective at reconstructing the characteristics of flow within the entire field. Simultaneous, multi-point measurements are possible with PIV, making it applicable to other areas, such as bifurcated or atherosclerotic vessel flow dynamics [6]. Because PIV implements digital image processing, the experimental set-up generally comprises an image input–output device, an image processing device and image processing software. The image input device, for which scanners, high-resolution charge-coupled device (CCD) cameras or camcorders are most commonly used (we opted for a CCD camera), serves to convert the images taken by the camera into a digital signal and supply them to

the image processing device. The image processing device carries out a variety of functions, such as archiving the input images onto the image board, detecting borders, thus determining the demarcation of the backgrounds, splitting the images into two halves and removing noise. The digital images of the field obtained by the image processing device usually represent the position of the particle in 2D space (x and y pixels) and the contrast (gray) value of each pixel.

The flow velocity algorithms can be divided into particle-tracing and gray value correlation methods. The particle-tracing method involves calculating the velocity vector by computing the velocity variances of the particles at 1-min intervals after locating the center of each particle. The particles are recognized as a series of contiguous images, i.e. we locate a specific particle and search for the candidate particle within the image after a certain time interval, given the fact that the velocity of the particle does not fluctuate significantly within a short time period. This method is time-consuming due to the complex calculations involved. The gray value correlation method involves calculating the velocity vectors by regarding the particle with the maximum autocorrelation coefficient or mutual correlation coefficient as the candidate particle on the basis of the intensity of the contrast values of the particles distributed within one or more frames in series. The tracing of velocity vectors is followed by removal and correction of erroneous vectors and flow visualization [6]. We used an Nd:YAG laser (Spectron Laser Systems Ltd., Rugby, UK) as the light source and a Flow Master 3 (LaVision Co., Göttingen, Germany) as the image input-processing device.

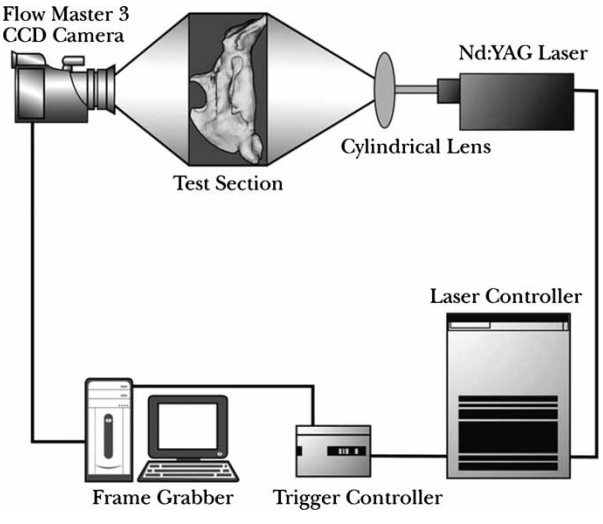

Figure 2. Experimental set-up.

Experiments involving PIV

A schematic outline of the flow visualization experiment within the nasal cavity is shown in Figure 2. The control system consists of 2 pulse light sources (150 mJ), an Nd:YAG laser, a CCD camera (LaVision Co.) with the capability of processing up to 4 pairs of paired images with a highest resolution of 1280×1023 pixels and a time interval of >1 μs, a trigger controller (LaVision Co.) for equalizing the camera and laser and a computer (LaVision Co.) that operates the whole process. The flow conduit model of the nasal cavity that traverses the flow-control bench is made up of five flowmeters serially connected to a tank. We used a spherical polyvinyl particle with a diameter of ≈ 80 μm as the tracing particle. The glycerol–water volume flow rate during the inspiratory and expiratory phases was set at 103 ml/s, corresponding to an airflow rate of 125 ml/s.

Results

Changes in flow within the nasal cavity during inspiration

The airflow that entered through the nasal vestibule collided with the anteroinferior part of the middle turbinate, producing a large degree of turbulence. The flow that branched off at the anterior end of the middle turbinate was divided between the middle and superior meatus. The flow passing the superior meatus had the highest velocity, followed by that in the middle and inferior meatus. There was some flow towards the olfactory area. In terms of the RMS average airflow velocity distribution, the most prominent fluctuation was noted at the anteroinferior part of the middle turbinate, indicating that this was the point with the highest velocity gradient. The flow passing into each pathway was measured as 17.5 ml/s in the superior meatus, 63.0 ml/s in the middle meatus and 38.0 ml/s in the inferior meatus, representing 14.7%, 53.2% and 32.1% of the total flow, respectively (Figure 3). The middle meatus was the main pathway used during the inspiratory phase.

Changes in flow within the nasal cavity during expiration

After the flow had passed through the nasopharynx it changed direction towards the nasal vestibule. Thus, a region of strong turbulence formed at the nasopharynx and moved into the nasal vestibule, forming a rapid velocity vector in the superior meatus. The fluctuation in the RMS average airflow velocity was noted to be most prominent

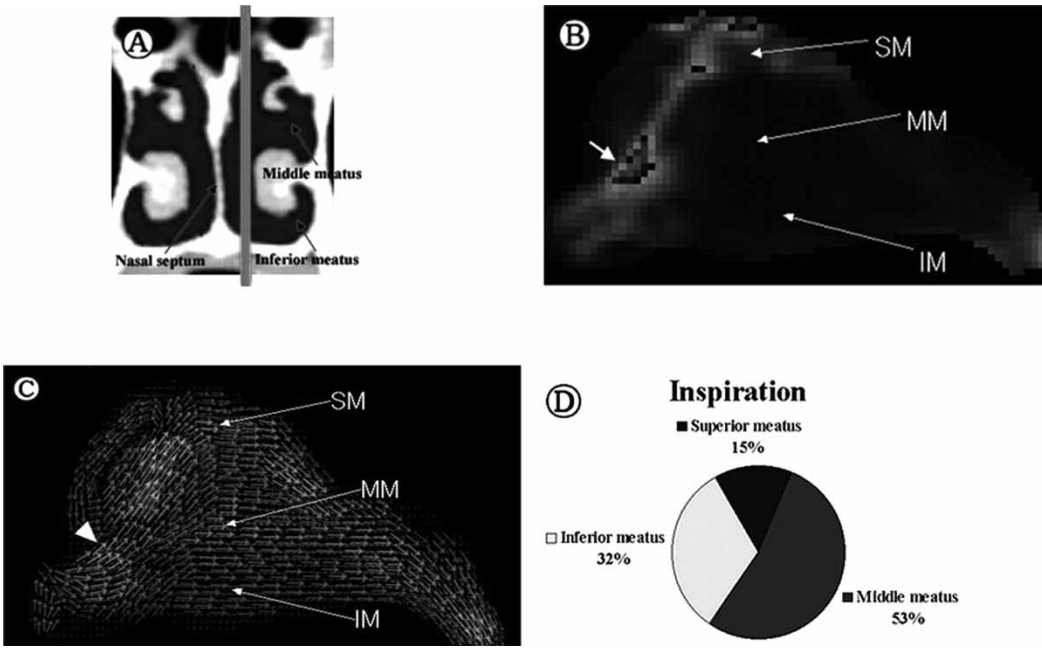

Figure 3. PIV results for inspiratory airflow in a plane parallel to the nasal septum, corresponding to an airflow rate of 125 ml/s. (A) Plane of airflow. (B) RMS average airflow velocity distribution. The arrow indicates the highest velocity gradient. (C) Mean velocity field. The arrowhead indicates counterclockwise turbulence at the anteroinferior part of the middle turbinate. (D) Flow rate distribution during inspiration. SM = superior meatus; MM = middle meatus; IM = inferior meatus.

at the nasopharynx, superior meatus and nasal vestibule. The airflow was measured at 50.4 ml/s in the inferior meatus, 52.2 ml/s in the middle meatus and 16.5 ml/s in the superior meatus, representing 42.3%, 43.8% and 13.9% of the total flow, respectively (Figure 4). The middle meatus was also the main pathway used during the expiratory phase. However, the amount of flow at the inferior meatus was larger than that during the inspiratory phase, because the flow collided with the nasopharyngeal wall as it passed through the nasal floor.

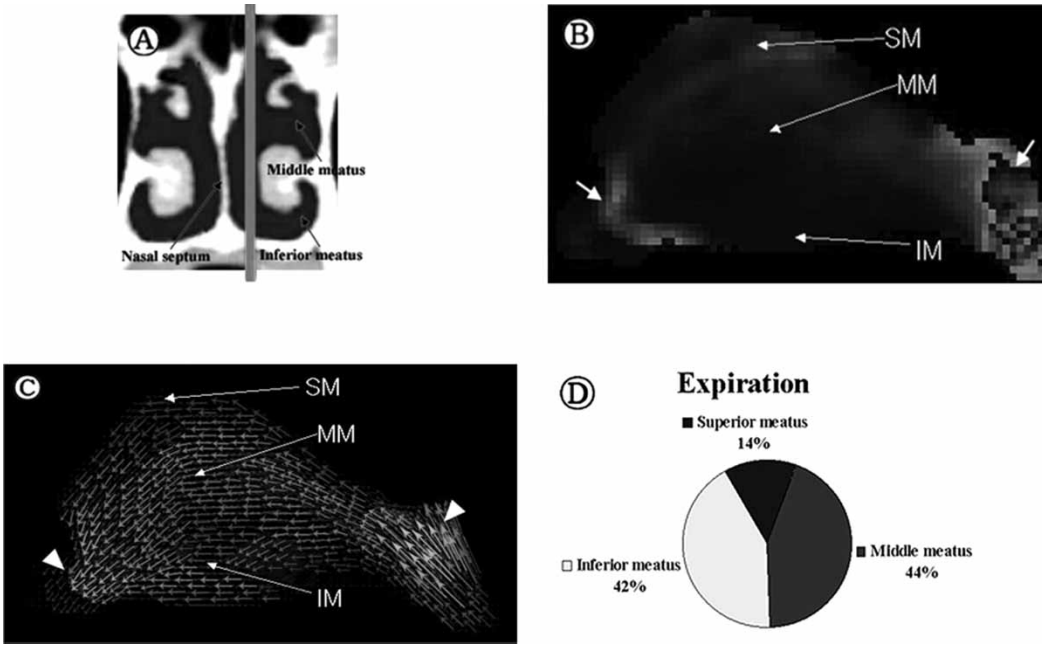

Figure 4. PIV results for expiratory airflow in a plane parallel to the nasal septum, corresponding to an airflow rate of 125 ml/s. (A) Plane of airflow. (B) RMS average airflow velocity distribution. The arrows indicate the highest velocity gradients. (C) Mean velocity field. The arrowheads indicate counterclockwise turbulence at the nasopharynx and near the vestibule. (D) Flow rate distribution during expiration. Abbreviations as in Figure 3.

Discussion

The status of the airflow within the nasal cavity provides the basis for physiological and pathological explanations of nasal disease. However, theoretical knowledge of the principles of aerodynamics may predict the flow at a certain point, albeit to a limited extent as the nasal cavity is such a complex structure that knowledge gained from aerodynamic studies is very inadequate. Investigations of the aerodynamics within the nasal cavity began to flourish in the 20th century. The main flow of air within the nasal cavity has been the subject of intense controversy. Various authors [1,7,8], using a variety of methods, concluded that the main flow of air occurs in the basement of the nasal cavity, and that the velocity and amount of flow are greatest at this point. By contrast, other authors [2,9–11] argued that the middle meatus is the main passage for airflow. The lack of agreement between these studies would seem to be the result of inaccurate modeling of the nasal cavity. Subsequently, Hopkins et al. [3] recreated the complex internal structure of the nasal cavity with a nasal model cast using a combination of rapid prototyping and solidification of clear silicone, and established PIV as an effective method for measuring flow. Kelly et al. [4], who studied detailed flow patterns in the nasal cavity utilizing this method, reported that there was very little flow in the olfactory slit and meatus, and that the highest flow velocities were observed at the nasal valve and in the inferior airway. In contrast, in our experiment, which was carried out using the same method as Kelly et al. [4], the main flow within the cavity, which was mostly laminar, passed through the middle meatus. These discrepancies are presumably due to differences in the structure of the inlet of the nasal cavity between the models, as well as anatomical variations.

During the inspiratory phase, $\approx$53.2% of the total inspired air passed through the middle meatus, which is in concordance with the report of Scherer et al. [2]. However, we also noted the occurrence of turbulent flow at a low velocity, which is in accordance with the result of Simmen et al. [11]. After the flow passes through the vestibule, it rotates towards the posterior direction and merges with the air from the anterior part of the middle turbinate, producing turbulent flow. Presumably this is in order to maximize the function of the nasal cavity as a heat converter. Although there is the possibility that turbulent flow will not occur, given the fact that the flow has just passed an area narrowed by the nasal valve during inspiration, the model could not simulate an active nasal valve due to technical limitations. Also, because turbulent flow allocates more air to the superior meatus and olfactory area, it is thought to facilitate olfactory function.

During the expiratory phase, a large area of turbulence is formed while the direction of flow changes from the nasopharynx to the nasal vestibule. The flow in the superior meatus moves into the nasal vestibule with the highest velocity. Of the total flow, 42.3% was through the inferior meatus and 43.8% through the middle meatus. It is presumed that the turbulent flow in this area is intensified by complex peri-nasopharyngeal structures such as the orifice of the Eustachian tube or the pharyngeal folds. The fact that the proportion of flow in the inferior meatus is higher during expiration than during inspiration is probably due to the formation of turbulent flow in the nasopharynx. After passing through the nasopharynx the flow of air is directed to the nasal vestibule, producing laminar flow. This is contrast to standard schematics proposed previously [12]. RMS average airflow velocity values were prominently large in the anteroinferior portion of the middle turbinate during inspiration and in the nasopharynx during expiration, which suggests that the fluctuation in flow velocity is significant in these regions, indicating the presence of turbulent flow.

Compared with previous methods using cadavers and casts, PIV is a new aerodynamic method which can be used to accurately model the anatomical complexity of the nasal cavity. Taking the current findings into account, one can assume that for severe septal deviation, which does not influence the main flow passing through the middle meatus, correction during septoplasty is not essential. Endoscopic sinus surgery performed at the middle meatus, which is currently popular, would also greatly enhance the airflow within the nasal cavity.

Further study is needed on the flow and pathological changes at each point within the nasal cavity, and to determine what sort of effect various forms of nasal surgery would have on the airflow within it. This will also help to determine the effect of hypertrophied tissue on air pressure and on the aerodynamically optimal tissue resection area.

Conclusions

We attempted to visualize the characteristics of flow, velocity at each point and the presence of turbulence in the nasal cavity using PIV, and obtained the following results: the majority of airflow within the nasal cavity occurs through the middle meatus, mostly in the form of laminar flow; and turbulent flow can be investigated at a physiological velocity. PIV is a good tool for estimating the aerodynamic properties of the nasal cavity.

References

[1] Hess MM, Lamprecht J, Horlitz S. Experimental study of airflow patterns in the human nasal model. Laryngol Rhinol Otol 1992;71:468–71.
[2] Scherer PW, Hahn II, Mozell MM. The biophysics of nasal airflow. Otolaryngol Clin North Am 1989;22:265–78.
[3] Hopkins LM, Kelly JT, Wexler AS, Prasad AK. Particle image velocity measurements in complex geometries. Exp Fluids 2000;29:91–5.
[4] Kelly JT, Prasad AK, Wexler AS. Detailed flow patterns in the nasal cavity. J Appl Physiol 2000;89:323–37.
[5] Miner CS, Dalton NN. Glycerol. New York: Reinhold; 1953. p. 280.
[6] Kim SG. A research on the PIV algorithm using image coding. Trans KSME 1999;24:153–60.
[7] Elad D, Liebenthal R, Weing BL, Einav S. Analysis of air flow patterns in the human nose. Med Biol Eng Comput 1993;31:585–92.
[8] Keyhani K, Scherer PW, Mozell MM. Numerical simulation of airflow in the human nasal cavity. J Biomed Eng 1995;117: 429–41.
[9] Hornung DE, Leopold DA, Yongentob SL. Airflow patterns in a human nasal model. Arch Otolaryngol Head Neck Surg 1987;113:169–72.
[10] Schreck S, Sullivan KJ, Ho CM, Chang HK. Correlations between flow resistance and geometry in a model of human nose. J Appl Physiol 1993;75:2273–87.
[11] Simmen D, Scherrer JL, Moe K, Heinz B. A dynamic and direct visualization model for the study of nasal airflow. Arch Otolaryngol Head Neck Surg 1999;125:1015–21.
[12] Proctor DF. Nasal physiology and defense of the lungs. Am Rev Respir Dis 1977;115:97–129.